NANO LETTERS

Letter

pubs.acs.org/NanoLett

Slurryless Li_2S/Reduced Graphene Oxide Cathode Paper for High-Performance Lithium Sulfur Battery

Chao Wang,[†,‡,§,∥] Xusheng Wang,[†] Yuan Yang,[⊥] Akihiro Kushima,[‡,§] Jitao Chen,*[,†] Yunhui Huang,*[,∥] and Ju Li*[,‡,§]

[†]Beijing National Laboratory for Molecular Sciences, College of Chemistry and Molecular Engineering, Peking University, Beijing, People's Republic of China

[‡]Department of Nuclear Science and Engineering and [§]Department of Materials Science and Engineering, Massachusetts Institute of Technology, Cambridge, Massachusetts 02139, United States

[∥]State Key Laboratory of Material Processing and Die & Mold Technology, School of Materials Science and Engineering, Huazhong University of Science and Technology (HUST), Wuhan, Hubei 430074, China

[⊥]Department of Mechanical Engineering, Massachusetts Institute of Technology, Cambridge, Massachusetts 02139, United States

Supporting Information

ABSTRACT: Lithium sulfide (Li_2S) is a promising cathode material for Li−S batteries with high capacity (theoretically 1166 mAh g^{-1}) and can be paired with nonlithium−metal anodes to avoid potential safety issues. However, the cycle life of coarse Li_2S particles suffers from poor electronic conductivity and polysulfide shuttling. Here, we develop a flexible slurryless nano-Li_2S/reduced graphene oxide cathode paper (nano-Li_2S/rGO paper) by simple drop-coating. The Li_2S/rGO paper can be directly used as a free-standing and binder-free cathode without metal substrate, which leads to significant weight savings. It shows excellent rate capability (up to 7 C) and cycle life in coin cell tests due to the high electron conductivity, flexibility, and strong solvent absorbency of rGO paper. The Li_2S particles that precipitate out of the solvent on rGO have diameters 25−50 nm, which is in contrast to the 3−5 μm coarse Li_2S particles without rGO.

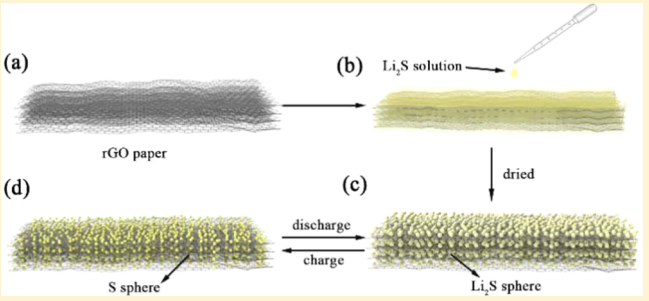

KEYWORDS: *Lithium sulfide, reduced graphene oxide paper, slurryless, flexible, nanoparticle*

Developing cheap and high energy density materials for electrochemical energy storage is of current interest.[1,2] Lithium sulfur (Li−S) battery is a promising candidate for next-generation energy storage devices.[3,4] For traditional Li−S battery systems, Li metal is used as the anode material.[5−7] However, lithium metal has safety and cyclability issues due to the formation of lithium dendrites;[8,9] the pulverized and detached lithium metal formed during cycling can result in explosions when exposed to air.[10,11] In view of this, lithium sulfide (Li_2S) has attracted much attention because safer anodes such as nanostructured silicon, aluminum, tin, graphene, transition metal oxides, and so forth can be paired with Li_2S, which do not have dendrite problem.[12,13] Li_2S has a high theoretical capacity of 1166 mAh g^{-1} and a high melting point of 938 °C.[14,15] However, two significant issues with the sulfur cathode, poor electrical conductivity and intrinsic polysulfide shuttle, also exist in Li_2S.[16,17] Furthermore, because Li_2S is highly sensitive to moisture and oxygen its handling is often more complex than pure sulfur and should be put in a protected atmosphere all of he time. Also, even though Li_2S should have better electrical conductivity than pure sulfur it is still essential to introduce additional electron conductors into Li_2S. Traditionally, this is done via the slurry approach, where the additional electron conductors (e.g., carbon), Li_2S, and binder powders are mixed into a slurry, and then doctor-bladed on solid aluminum foil and baked. But the slurry has relatively poor electron conductivity and mechanical properties. Uniform dispersion of Li_2S into a natively more conductive and flexible long-range 2D framework, like a macroscopic piece of paper, could be an effective way to utilize Li_2S in Li−S batteries.

Recently, a number of studies on Li_2S with promising results have emerged. Some ball-milled commercial Li_2S to get different particle sizes, and the resulting particles are mostly micrometer-sized.[12−15,18] If the Li_2S particle is coarse sized, there may be an energy/voltage barrier in the initial charge process, and the rate capability and the cyclability might be poor. But if the particle size decreases to nanoscale, the barrier will be much smaller as indicated by the initial cyclic voltammetry (CV) curve and charge profile. There are already some reports about nanosized Li_2S that achieved good results. Very recently, there are also some impressive results about

Received: November 24, 2014

DOI: 10.1021/acs.nanolett.5b00112
Nano Lett. XXXX, XXX, XXX−XXX

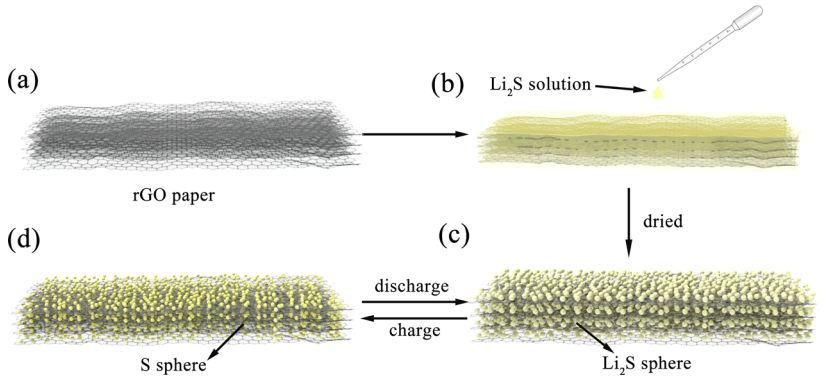

Figure 1. Schematic illustration of the material preparation processes of the nano-Li_2S/rGO paper and structure changes during cycling of nano-Li_2S/rGO paper. (a) The rGO paper was obtained by freeze-drying of GO suspension in water at −50 °C first and then reduced by heat treatment under 5% H_2/Ar atmosphere, and the rGO paper is flexible and has good in-plane electrical conductivity (3.07×10^4 S/m). (b) Drop coating of the rGO paper by the solution of Li_2S in anhydrous ethanol in the glovebox. Moisture and oxygen in the glovebox were less than 1 ppm. (c) The final product, nano-Li_2S/rGO paper, after removing the free and crystallized ethanol by vacuum heating at 300 °C for 2 h. Li_2S particles were uniformly distributed throughout the rGO paper. (d) Schematic shows the possible charge situation of the nano-Li_2S/rGO paper; sulfur is smaller than Li_2S. The rGO paper can tolerate the volume change during cycling and remains stable.

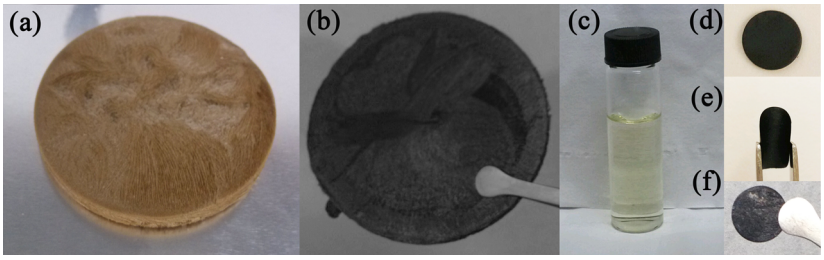

Figure 2. Photograph of the GO gel after freeze-drying in a Petri dish (a), the rGO paper after heat treatment of the pressed GO gel (b), and solution of Li_2S in anhydrous ethanol and the concentration is 15 mg mL^{-1} (c). The disk of rGO paper with a diameter of 11 mm: (d) top view, (e) bent rGO paper, indicating it has a good flexibility, (f) the nano-Li_2S/rGO paper synthesized by the drop coating method.

graphene oxide (GO) and nano-Li_2S composites.[19−21] However, these processes all involved synthesizing GO and Li_2S powders, which are made into viscous slurry after mixing with binders, then cast on solid aluminum foil to make the cathode of coin cell. These processes all need to be performed in protective atmosphere due to the sensitive nature of Li_2S. Nan et al. used a solution reaction method to form Li_2S and could control the size of the Li_2S particles by changing the concentration of solution and reaction time.[22] This method is effective to get nanosized Li_2S. They then carbon coated the Li_2S spheres by the chemical vapor deposition (CVD) method. However, all these multistep processes, including the CVD, were done in a glovebox to protect the Li_2S from moisture and oxygen. Wu et al. explored a method using the freshly precipitated Li_2S nanoparticles with polymer coating to avoid agglomeration.[23] Then they annealed the material at 700 °C under Ar atmosphere. The carbon coated Li_2S nanoparticles have a diameter around 10 nm and exhibited good electrochemical performance. But the multistep synthesis and electrode production still need to be protected in an inert atmosphere. Generally speaking, the pathways had been very similar to preparing sulfur cathode, just changing sulfur to Li_2S; but the equipment requirements for industrial scale up would be more stringent than dealing with pure sulfur cathode (in the pure sulfur cathode case, however, the gas-sensitivity challenge is transferred to the lithium metal anode side).

We have developed a much easier pathway of material synthesis and electrode preparation. The result is a flexible nano-Li_2S/reduced graphene oxide (nano-Li_2S/rGO) cathode paper that can be used directly as cathode to be paired with safer anode materials such as silicon, aluminum, tin, graphene, transition metal oxides, and so forth. It means we can skip the usual steps of making viscous slurry and applying them to the metal substrate in battery assembly.

The reduced graphene oxide (rGO) paper was prepared by freeze-drying graphene oxide (GO), which was then reduced in a heat treatment (Figure 1a). The nano-Li_2S loading is achieved by drop coating using anhydrous ethanol as the solvent, as Li_2S is very soluble in ethanol (Figure 1b). More uniform distribution of Li_2S in the network is expected to exhibit a superior electrochemical performance. The rGO paper has a strong solvent absorbency, so the Li_2S solution can infiltrate throughout the rGO paper and the Li_2S particle precipitates are distributed very homogeneously inside the rGO paper. All the processes are illustrated in Figure 1. This material preparation pathway is very easy (but still in a protected atmosphere) and does not use high temperature (just between room temperature and 300 °C). Simple, lower temperature and scalable processing is essential for industrial scale-up, especially if the protected atmosphere is a given. To our surprise, after the very simple process of ethanol evaporation under a vacuum, the precipitated Li_2S particles are nanosized spheres. The flexible rGO paper prevents the agglomeration of Li_2S particles and also can accommodate the stress caused by the large volume change during lithiation and delithation (Figure 1c,d).[24] Moreover, the long-range rGO network, just like a macroscopic piece of paper, is quite conductive and mechanically stable during cycling.[25]

DOI: 10.1021/acs.nanolett.5b00112
Nano Lett. XXXX, XXX, XXX−XXX

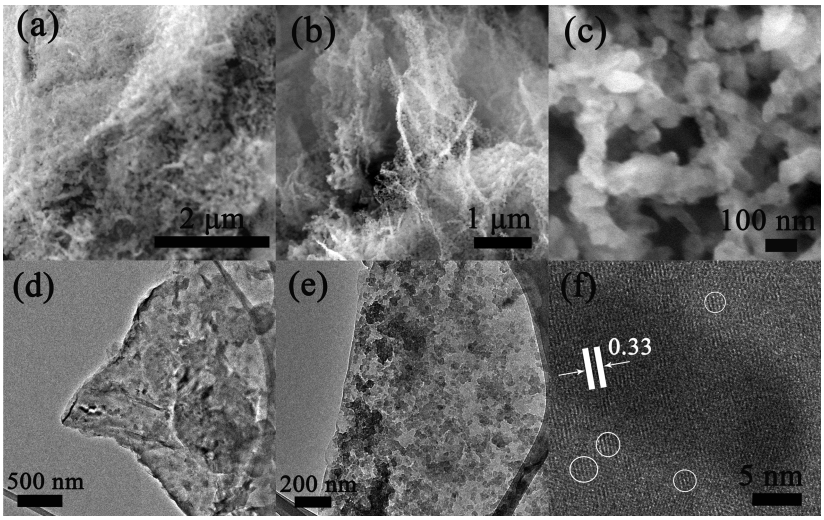

Figure 3. SEM and TEM images of the nano-Li_2S/rGO paper. (a) Top view of the nano-Li_2S/rGO paper, (b) side view of the Li_2S/rGO paper, and (c) the Li_2S particles at high magnification; (d,e) TEM images of the nano-Li_2S/rGO paper, and (d) is the overlap of many layers. There are many small crystals on the graphene surface as seen in (f), which is smaller than 10 nm. The nano-Li_2S/rGO paper was cut into small piece and use as SEM samples directly. TEM samples were prepared by sonicating a small piece of nano-Li_2S/rGO paper in hexane for 5 min; then a lacy carbon mesh was used to immerse into the dispersion and take out to put on the TEM holder as soon as possible to try to reduce the degree of oxidation of Li_2S. As the sonicating time is short, there may be some thick samples on the mesh.

GO was prepared via the same method as in our previous studies.[26] Figure 2a shows the GO aerogel after freeze-drying of the ice solid under vacuum for 48 h. The GO aerogel was pressed into paper form, and annealed at 800 °C for 4 h under 5% H_2/Ar atmosphere. The obtained rGO paper (Figure 2b) was cut into discs, which are very flexible as shown in Figure 2d,e (also can be seen from the movie in the Supporting Information). The Li_2S solution is clear and transparent, as shown in Figure 2c. The final nano-Li_2S/rGO paper (Figure 2f) can be directly used as the cathode electrode in coin cells without aluminum current collector or binder, which saves much weight. The material preparation processes and morphology are very sensitive to moisture and oxygen, so all the processes involving Li_2S were done in a glovebox with moisture and oxygen concentrations below 1 ppm. Details of the procedure are shown in Supporting Information.

We first check whether the pressed rGO paper is a good enough conductive support. The electrical conductivity was measured by a four-probe setup. The sheet resistance of the rGO paper is 0.65 Ω/sq, and the in-plane electrical conductivity is 3.07×10^4 S/m, which is similar to previously reported result.[27] Details of the calculation are presented in the Supporting Information. This is much better than the electrical conductivity of a typical baked slurry (~10^2 S/m) and is already good enough to be used as the electrode directly if the electrode size is approximately in centimeters, like for the coin cells we demonstrate below. For still larger-area electrodes, a sparse aluminum wire net (pore size ~ centimeter) may be padded beneath our freestanding cathode paper to improve long-range electron transport in-plane. In contrast, the traditional slurry approach must use a solid foil and cannot use a metal wire net because of the viscous nature of the slurry, as the solid aluminum foil serves both an electrical role and a mechanical role during doctor-blading and cycling of the slurry.

We used the nano-Li_2S/rGO disc directly as the electrode after the ethanol dried in a vacuum without heat treatment. The cells using such untreated paper showed very poor performance: the capacity was nearly zero. After doing thermogravimetric analysis (TGA), we found that there was weight loss at low temperature. Supporting Information Figure S1 shows the TGA curves of the precipitated Li_2S powder before and after heat treatment. The unheated sample had been put under a vacuum overnight. We found that there was nearly 50 wt % weight loss if the unheated Li_2S powder is annealed at 200 °C. We think this loss may be mainly due to the decomposition of solvated compound of Li_2S with ethanol ($Li_2S{\cdot}CH_3CH_2OH$) formed during precipitation from ethanol. It appears that $Li_2S{\cdot}CH_3CH_2OH$ is electrochemically inactive, while the decomposition product Li_2S after 200 °C annealing is electrochemically active.

We checked the XRD diffraction of the powder before heat treatment, which is shown in Supporting Information Figure S2. We can see the main peaks of Li_2S (shown in red stars) from the diffraction, but there are some other peaks that we can hardly attribute to any crystal, indicating that the powder is not pure Li_2S. We then heated the powder to 300 °C to bake out the residual ethanol. The TGA curves of the heat-treated powder shows that there was nearly no weight loss after 200 °C, which indicates that ethanol has been fully removed (Supporting Information Figure S1). The XRD diffraction of the nano-Li_2S/rGO paper after thermal treatment is shown in Supporting Information Figure S3. The XRD diffraction of Li_2S (JCPSD No.65-2981) and the pure rGO paper are also shown in Supporting Information Figure S3. We can see a high peak for the rGO paper centered around $2\theta = 26°$, which is mainly due to the graphitization of graphene oxide after thermal treatment at 800 °C. The highest peak of Li_2S is at $2\theta = 26.98°$, which nearly overlaps with the rGO peak, and the other peaks match well with the PDF data. The peaks are not very sharp, indicating that the precipitated Li_2S is not well crystallized.

SEM and TEM was used to investigate the morphology of the nano-Li_2S/rGO paper. Figure 3 displays the SEM (a,b,c) and TEM (d,e,f) images of the nano-Li_2S/rGO paper. Supporting Information Figure S5 shows the top views of the nano-Li_2S/rGO paper at low magnification. The images shows some material covering the surface of the rGO paper. When we

DOI: 10.1021/acs.nanolett.5b00112
Nano Lett. XXXX, XXX, XXX−XXX

use higher magnification, we can see many particles uniformly distributed on the graphene layers (Figure 3a). We find that the particles are smaller than 100 nm (Figure 3c). Figure 3b shows the edges of the nano-Li_2S/rGO paper, which were cut by scissors when preparing the SEM sample. We can see the inner space of the nano-Li_2S/rGO paper, which indicates that Li_2S nanoparticles are also distributed uniformly between the graphene layers. For the purpose of contrast, the SEM images of Li_2S powder precipitated without rGO paper, as the control sample, are shown in Supporting Information Figure S6. The primary Li_2S particles are small (Supporting Information Figure S6b) but they are agglomerated to form secondary particles around 3−5 μm in diameter. Therefore, the rGO paper provides nucleation and anchoring sites for the precipitated Li_2S nanoparticles and prevent the agglomeration of Li_2S.

Supporting Information Figure S7 shows the TEM image of the rGO sheet. We can see that the surface of the rGO sheet is very clean and the sheet is very thin. Figure 3d−f shows the TEM images of sheets of nano-Li_2S/rGO paper. From Figure 4d,e, we can see that there are many nanoparticles on the rGO

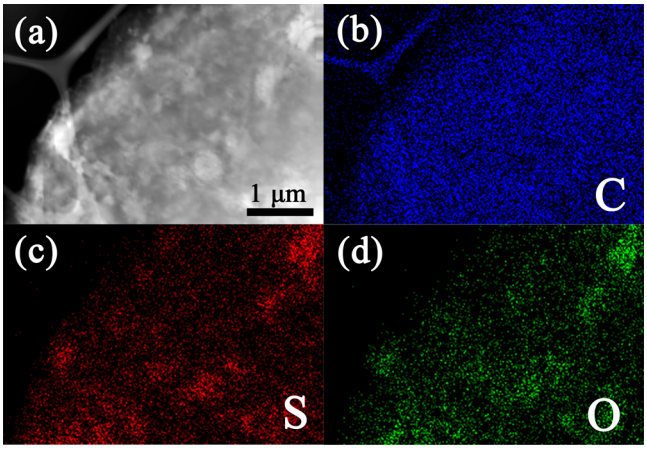

Figure 4. HAADF-STEM image (a) and corresponding EDS mapping for the element distribution in nano-Li_2S/rGO paper: (b) C, (c) S, and (d) O.

sheet. Figure 4d is relatively thick, and we can hardly identify each particle because the image has many overlapping layers. As shown in Figure 3e, the Li_2S spheres are in diameter about 25−50 nm. Figure 3f shows the high resolution of the Li_2S sphere, the interlayer distance is 0.33 nm, which is consistent with the (111) plane spacing of Li_2S. Moreover, we found that there are many crystal fringes on the graphene sheet as shown in Figure 3f, and the distance is also 0.33 nm. We assume that it is because small Li_2S crystals are distributed all over the surface of graphene sheet, and the crystal size is less than 5 nm.

In order to further identify the microstructure of the nano-Li_2S/rGO paper, high-angle annular dark-field scanning transmission electron microscopy (HAADF-STEM) and the corresponding EDS mapping were used, as shown in Figure 4. The HAADF-STEM image (Figure 4a) further illustrates that there are many particles on the graphene sheets. The selected area is relatively thick and has many graphene sheets. The elemental maps of C, S, and O clearly demonstrate that they are homogeneously distributed in the nano-Li_2S/rGO paper. The appearance of O is mainly from the oxygen of rGO and the oxidation of Li_2S during the TEM sample preparing processes. X-ray photoelectron spectroscopy (XPS) of C 1s, S 2p, O 1s, and Li 1s for the nano-Li_2S/rGO paper are shown in Supporting Information Figure S4. The fitting results show the sample had partially oxidized during the transport to XPS chamber. The peaks of the S 2p at 160.94 and 159.56 eV can be ascribed to Li_2S.[28] Combined with the S 2p and C 1s spectra, we see there are some interactions between S and C. The subpeaks of S at 162.22 eV and C at 284.68 eV can be ascribed to the C−S bond in the nano-Li_2S/rGO paper, indicating that some sulfur atoms may be bonded to the rGO.[17,29] These C−S bonds anchor the 25−50 nm Li_2S nanoparticles to rGO, prevent their agglomeration, and provide stability during lithiation/delithiation.

The electrochemical properties of our cathode paper were evaluated using coin cells with lithium metal as the anode and Celgard 2400 film as the separator. The cathode paper disc has diameter 11 mm and nano-Li_2S loading of about 0.8−1.5 mg cm^{-2}. Electrolyte solution with polysulfide additive was prepared by mixing a small amount of sulfur and lithium sulfide powder into the electrolyte and stirring overnight. The as-synthesized solution has a nominal molecular formula of Li_2S_8 and the concentration of Li_2S_8 is 0.01 M. The amount of electrolyte we used in the coin cell is 15 μL, so the total amount of sulfur in the polysulfide additive electrolyte was less than 4 wt % (0.038 mg) of that in the nano-Li_2S/rGO paper electrode. This indicates that the majority of the capacity originates from Li_2S and the electrolyte can give a capacity no more than 38 mAh g^{-1} (assuming that sulfur has a reversible capacity of 1000 mAh g^{-1}). Cells were galvanostatically and potentiostatically charged and discharged between 1.7 and 2.8 V versus Li^+/Li on a Land CT2001A battery tester except for the first cycle, which were charged at 0.05 C to 3.6 V and discharged to 1.8 V versrus Li/Li^+ throughout the text.

Figure 5a shows the cyclic voltammetry (CV) curves of the nano-Li_2S/rGO paper in the first five cycles. It has been reported that the charge barrier is universal in Li_2S, so we scanned to 3.6 V at the first cycle to see if there are some uncommon peaks.[14] Figure 5a displays the first cycle of the CV curve. It is obvious that there are two anodic peaks for nano-Li_2S/rGO paper in the initial sweep. The anodic peak centered around 2.5 V can be attributed to the oxidation of Li_2S to S. The other small peak at 3.54 V may be caused by the agglomeration of Li_2S nanoparticles, which has been reported in the literature.[14,30] The peak at 3.5 V is very small, which means the volume fraction of the agglomerated Li_2S large particles is small. It is clear there is no obvious initial energy/voltage barrier for nano-Li_2S/rGO paper, even though these barriers usually are seen if one uses micron-sized Li_2S particles. The appearance of the energy/voltage barrier at the first cycle is mainly due to the low electrochemical activity of bulk Li_2S, and the barrier can be decreased by charging at low rate. Here, we assume that the nanostructuring and the polysulfide additive reduce the barrier or even eliminate the barrier. There are some reports about the utilization of nanosized Li_2S with the combination of polysulfide additive for Li−S batteries. Han et al. reported a Li_2S-reduced graphene oxide nanocomposite, although they did not give the CV curves, we can see from the dQ/dV curves that there is no initial energy barrier.[31] The same situation can also been found in the study of Wu et al.;[23] we can see that the C−Li_2S nanocomposite has no obvious energy barrier from their charge profile of the first cycle.

There are two redox peaks in the first cycle of CV, and the two cathodic peaks are due to the multiple reduction of sulfur in the presence of Li^+ ions. The peak at 2.3 V is related to the

DOI: 10.1021/acs.nanolett.5b00112
Nano Lett. XXXX, XXX, XXX−XXX

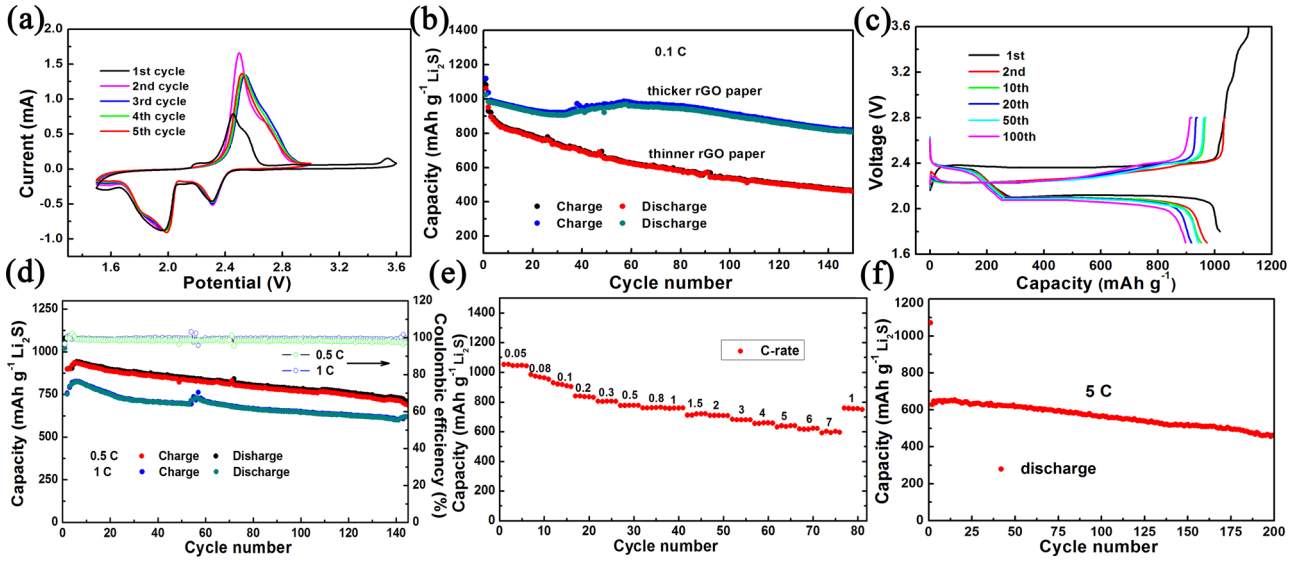

Figure 5. (a) Cyclic voltammograms of the nano-Li_2S/rGO paper electrode between 1.5 and 3.6 V at the first cycle and the following four cycles scan between 1.5 and 3 V at a potential scanning rate of 0.2 mV s^{-1}. Electrochemical characteristics of the nano-Li_2S/rGO paper electrodes. All electrodes were charged to 3.6 V at the first cycle in 0.05 C rate and then cycled between 1.7−2.8 V. Electrolyte was 0.6 M LiTFSI with the additive of 0.01 M Li_2S and 0.4 M $LiNO_3$. (b) Cycling performance of the thicker and thinner nano-Li_2S/rGO papers at a current rate of 0.1 C. (c) Charge and discharge profiles of the thicker nano-Li_2S/rGO paper at the 1st, 2nd, 10th, 20th, 50th, 100th cycle at 0.1 C. (d) Cycling performance and corresponding Coulombic efficiency at current rates of 0.5 and 1 C for the thicker nano-Li_2S/rGO paper. (e) Rate performance of the nano-Li_2S/rGO paper electrode with a current rate ranging from 0.05 to 7 C. (f) Cycling performance of the nano-Li_2S/rGO paper electrode at high current rate of 5 C.

reduction of S_8 to long chain lithium polysulfides. The following peak around 2 V is associated with the further reduction of long chain lithium polysulfides to Li_2S_2 and Li_2S. The cathodic peaks overlap in the subsequent four cycles (Figure 5b). Compared with the first cycle, the anodic peaks have shifted slightly to a higher voltage and the intensities have increased very much. The redox peaks stay nearly the same from the third to the fifth cycles, indicating a good electrochemical reversibility of the nano-Li_2S/rGO paper.

During the material preparation process, we found that pretreatment in an oven at 80 °C for 2 days before annealing can produce a much thicker rGO paper, which is more flexible and has a better solvent absorbency (see movie in Supporting Information). The thinner one was heat-treated soon after freeze-drying. After freeze-drying, the GO gel is very difficult to handle because it is fragile and brittle, but after the 80 °C preheating, the structure becomes much tougher and easier to handle. The quality of the as-prepared rGO disks is around 0.6−1 mg and the loading of Li_2S is about 0.8−1.5 mg, which indicates that the Li_2S content is about 50−60 wt % in the electrode. The thinner and thicker rGO disks have the similar Li_2S loading by weight.

The electrochemical performance of the thicker and thinner nano-Li_2S/rGO papers were studied. Figure 5b shows the cycling performance of the two kinds nano-Li_2S/rGO papers at a low rate of 0.1 C. We can see that the discharge capacities at the first cycle of the thicker and thinner samples are 1119 and 1060.7 mAh g^{-1} (based on Li_2S), respectively, which is very high and among the best reported values.[14,15,30] Except for the fast fading of capacity for both the thicker and thinner cathode paper in the first cycle, the thicker cathode paper shows a much better electrochemical performance than the thinner one. After 150 cycles, the capacity of the thicker cathode paper still maintains at 816.1 mAh g^{-1}, indicating that the capacity fading rate is 0.18% per cycle. The thinner cathode paper has a capacity of 465.4 mAh g^{-1} after 150 cycles with a fading rate of 0.3% per cycle. The capacity retention of the thicker cathode paper is much better than the thinner one but even the performance of the thinner one is better than that of most reports.[14,31] Because we do not use aluminum foil or binder, the weight percentage of active Li_2S material in the whole cathode is much higher than reports using traditional slurry-on-metal-foil electrodes. The BET surface area of the thinner and thicker rGO paper are similar and are all around 185 m^2 g^{-1}, which is small compared to porous carbon materials. Here, we propose that the solvent absorption ability of rGO directly affect the electrochemical performance. A highly wettable rGO absorbs the electrolyte and traps the dissolved polysulfides during cycling. The solvent absorbency of the rGO paper is good, as shown in the movie in Supporting Information, and the thicker rGO paper is better than the thinner one, which may be the main reason for the better cyclability of the thicker paper.

The corresponding charge and discharge profiles of the thicker nano-Li_2S/rGO paper at the rate of 0.1 C is shown in Figure 5c. The charge and discharge plateaus stay nearly the same during cycling except for the first charge profile, which is around 2.4 V and corresponds to the oxidization process of Li_2S. The following small plateaus between 3.2 and 3.6 V, which are consistent with the CV results, may be caused by the agglomeration of Li_2S nanoparticles or the oxidation of electrolyte. Two discharge voltage plateaus appear at around 2.35 and 2.1 V, which can be assigned to the two-step reaction during discharge process, and are consistent with the typical discharge profile of sulfur cathodes. The voltage plateaus changed very little since the second cycle, as the current rate in the first cycle is 0.05 C and followed by 0.1 C during cycling. Even after 100 cycles, the charge and discharge profiles stay nearly the same, indicating that the nano-Li_2S/rGO paper has excellent capacity retention. Compared with the recent research

DOI: 10.1021/acs.nanolett.5b00112
Nano Lett. XXXX, XXX, XXX−XXX

of C−Li_2S composite that shows good performance, the voltage polarization in our sample is smaller.[30]

The electrochemical performance in the following paragraphs are based on the thicker cathode paper. Figure 5d shows the cycling performance of the nano-Li_2S/rGO paper at 0.5 and 1 C rate. Beyond the first cycle under 0.05 C, which achieves charge and discharge capacities above 1000 mAh g^{-1}, the discharge capacity at 0.5 and 1 C are 897.7 and 752.2 mAh g^{-1}, respectively. The discharge capacities still remain at 692 and 617.6 mAh g^{-1} after 145 cycles, which demonstrates that the capacity retentions are 77.1 and 82.1%, respectively. The discharge capacity at the 100th cycle is 771.3 mAh g^{-1} at 0.5 C rate, which is equal to 1102 mAh g^{-1} of sulfur. This result is among the best reported for lithium sulfur battery. Wu et al. reported a discharge capacity of 1200 mAh g^{-1} after 100 cycles under 0.5 C of the C−Li_2S nanocomposite. Compared to their results, we have higher active material loading on the electrode. (Their loading is less than 30 wt % including the aluminum foil.[23]) The Coulombic efficiency of the nano-Li_2S/rGO paper is around 98−99% during the cycling, and the high Coulombic efficiency during cycling can be attributed to the effect of adding $LiNO_3$ and polysulfide into the electrolyte and the good entrapment of polysulfides inside the rGO paper.

The rate capability of the nano-Li_2S/rGO paper at various rates from 0.05 to 7 C is shown in Figure 5e. The nano-Li_2S/rGO paper exhibits excellent rate performance with discharge capacities of 1044, 916, 758, 708, and 640 mAh g^{-1} at 0.05, 0.1, 1, 3, and 5 C, respectively. Even at a high rate of 7 C, it still achieves a high reversible capacity of 597 mA g^{-1}. The rate capability is significantly higher than those reported for Li_2S composite of Li−S batteries in the literatures. Moreover, after cycling at such a high rate the capacity recovered to 755 mAh g^{-1} at 1 C, implying a good reversibility of the nano-Li_2S/rGO paper. The corresponding charge and discharge profiles at different C-rates are presented in Supporting Information Figure S8. We can see that the polarization of the charge and discharge plateaus were increased slowly especially at low rate, which is much better when compared with the literatures.[23,30,31] Even at 1 C, the plateaus change very little from 0.05 C. Figure 5f shows the cycling performance of the nano-Li_2S/rGO paper at a high current rate of 5 C. We can see that the discharge capacity can still remain at 462.2 mAh g^{-1} after 200 cycles.

Electrochemical impedance spectroscopy (EIS) was used to examine the nano-Li_2S/rGO paper (Supporting Information Figure S9). The intercept on Z_{real} axis in the high-frequency region corresponds to the resistance of the electrolyte (R_s). The resistance of the electrolyte is very small, less than 5 Ω. The semicircle in the high-frequency region before cycling reflects the out-of-plane charge transfer resistance (R_{ct}), which is related to the electrode/electrolyte interface. The oblique inclined line in the low-frequency region represents the Warburg impedance (Z_w), which is related to the solid-state diffusion of Li ions in the electrode materials. In the Nyquist plots obtained after running for 150 cycles using the same coin cell, a new semicircle appears in the high-frequency range, which may be mainly due to the formation of a passivation film on the electrode. We hypothesize that the passive film should be the deposition of Li_2S on the surface of the nano-Li_2S/rGO paper. The R_{ct} values of the nano-Li_2S/rGO paper before and after cycling were around 219 and 53 Ω, respectively. The total resistance after cycling is about 163 Ω, which decreased a little bit after cycling. This could be due to the good accommodation between graphene and Li_2S nanoparticles after several cycles and we think that the interaction between the Li_2S nanoparticles and graphene may have become stronger than the initial adhesion.

We then disassembled the coin cell after cycling 150 times and the SEM images are shown in Supporting Information Figure S10. We can see that the structure of the nano-Li_2S/rGO paper is well maintained after 150 cycles. There are no obvious cracks on the electrode, and the surface of the electrode seems smoother than the fresh one before cycling. This indicates the Li_2S/S nanoparticles are well-anchored on the rGO during cycling. The Li_2S layer should be thin as we can still clearly see the graphene layers below. Here, the electrode is demonstrated to be very stable and the active nanoparticles do not lose contact with rGO during cycling. Thus, the nano-Li_2S/rGO paper electrode shows excellent rate capability and long cycle life even at very high currents.

In summary, we have developed a simple drop coating method in protective atmosphere to synthesize a free-standing and binder-free Li_2S/rGO cathode paper for Li−S batteries without the use of viscous slurry and metal substrate, which leads to significant weight savings. To our surprise, with such an easy slurryless method we can synthesize nanosized Li_2S particles as small as 25−50 nm and distribute them uniformly inside the long-range interconnected rGO paper. The flexible and conductive paper electrode shows excellent cycling life and rate capability with a reversible discharge capacity of 816.1 mAh g^{-1} after 150 cycles at 0.1 C, and 597 mAh g^{-1} even at 7 C. After cycling 200 times at 5 C, the capacity can still remain at 462.2 mAh g^{-1}. The superior electrochemical performance may be attributed to the following reasons: (1) the nanosized Li_2S particles could decrease the energy barrier for Li ions transport; (2) the uniform distribution of Li_2S nanoparticles in the rGO framework can improve the utilization of Li_2S; (3) the good solvent absorbency of rGO paper can confine polysulfides between the graphene layers and alleviate the capacity loss during cycling; and (4) the interconnected conductive rGO paper can facilitate transportation for both electrons and Li ions. Moreover, the flexible nano-Li_2S/rGO paper can accommodate the stress generated from the large volume change during charge and discharge, so as to maintain the mechanical integrity of the electrode, which is very important for cyclability.

■ ASSOCIATED CONTENT

Ⓢ Supporting Information

Additional information for methods used for materials preparation and electrochemical measurement and additional figures depicting experimental results. Two recorded movies to support the flexibility and solvent absorbency of rGO paper. This material is available free of charge via the Internet at http://pubs.acs.org.

■ AUTHOR INFORMATION

Corresponding Authors

*(J.C.) E-mail: chenjitao@pku.edu.cn.
*(Y.H.) Email: huangyh@mail.hust.edu.cn.
*(J.L.) Email: liju@mit.edu.

Notes

The authors declare no competing financial interest.

DOI: 10.1021/acs.nanolett.5b00112
Nano Lett. XXXX, XXX, XXX−XXX

■ ACKNOWLEDGMENTS

The authors gratefully acknowledge the financial support by the Qinghai Province Science and Technology program (2012-G-Y28, 2014-ZJ-948), the National Basic Research Program of China (973 Program) (Grant 2014CB660806). They are also grateful to Dr. Peng Bai of MIT, Department of Chemical Engineering, for valuable discussion. The support by the China Scholarship Council (CSC) during a one year visit of Chao Wang to MIT is acknowledged. J.L. acknowledges support by NSF DMR-1120901.

■ REFERENCES

(1) Tarascon, J. M.; Armand, M. *Nature* **2001**, *414*, 359−367.
(2) Choi, N. S.; Chen, Z. H.; Freunberger, S. A.; Ji, X. L.; Sun, Y. K.; Amine, K.; Yushin, G.; Nazar, L. F.; Cho, J.; Bruce, P. G. *Angew. Chem., Int. Ed.* **2012**, *51*, 9994−10024.
(3) Yang, Y.; Zheng, G.; Cui, Y. *Chem. Soc. Rev.* **2013**, *42*, 3018−3032.
(4) Manthiram, A.; Fu, Y.; Chung, S.; Zu, C.; Su, Y. *Chem. Rev.* **2014**, *114*, 11751−11787.
(5) Duan, B.; Wang, W.; Wang, A.; Yu, Z.; Zhao, H.; Yang, Y. *J. Mater. Chem. A* **2014**, *2*, 308−314.
(6) Wang, C.; Wan, W.; Chen, J.; Zhou, H.; Zhang, X.; Yuan, L.; Huang, Y. *J. Mater. Chem. A* **2013**, *1*, 1716−1721.
(7) Zhang, S. S.; Read, J. A. *J. Power Sources* **2012**, *200*, 77−82.
(8) Ding, F.; Xu, W.; Graff, G. L.; Zhang, J.; Sushko, M. L.; Chen, X.; Shao, Y.; Engelhard, M. H.; Nie, Z.; Xiao, J.; Liu, X.; Sushko, P. V.; Liu, J.; Zhang, J. G. *J. Am. Chem. Soc.* **2013**, *135*, 4450−4456.
(9) Zheng, G. Y.; Lee, S. W.; Liang, Z.; Lee, H. W.; Yan, K.; Yao, H. B.; Wang, H. T.; Li, W. Y.; Chu, S.; Cui, Y. *Nat. Nanotechnol.* **2014**, *9*, 618−623.
(10) Besenhard, J. O.; Yang, J.; Winter, M. *J. Power Sources* **1997**, *68*, 87−90.
(11) Chandrashekar, S.; Trease, N. M.; Chang, H. J.; Du, L. S.; Grey, C. P.; Jerschow, A. *Nat. Mater.* **2012**, *11*, 311−315.
(12) Hassoun, J.; Scrosati, B. *Angew. Chem., Int. Ed.* **2010**, *49*, 2371−2374.
(13) Yang, Y.; McDowell, M. T.; Jackson, A.; Cha, J. J.; Hong, S. S.; Cui, Y. *Nano Lett.* **2010**, *10*, 1486−1491.
(14) Yang, Y.; Zheng, G.; Misra, S.; Nelson, J.; Toney, M. F.; Cui, Y. *J. Am. Chem. Soc.* **2012**, *134*, 15387−15394.
(15) Cai, K.; Song, M.; Cairns, E. J.; Zhang, Y. *Nano Lett.* **2012**, *12*, 6474−6479.
(16) Manthiram, A.; Fu, Y.; Su, Y. *Acc. Chem. Res.* **2012**, *46*, 1125−1134.
(17) Wang, D.; Zeng, Q.; Zhou, G.; Yin, L.; Li, F.; Cheng, H.; Gentle, I. R.; Lu, G. Q. M. *J. Mater. Chem. A* **2013**, *1*, 9382−9394.
(18) Hayashi, A.; Ohtsubo, R.; Ohtomo, T.; Mizuno, F.; Tatsumisago, M. *J. Power Sources* **2008**, *183*, 422−426.
(19) Seh, Z. W.; Wang, H.; Liu, N.; Zheng, G.; Li, W.; Yao, H.; Cui, Y. *Chem. Sci.* **2014**, *5*, 1396−1400.
(20) Zhang, K.; Wang, L.; Hu, Z.; Cheng, F.; Chen, J. *Sci. Rep.* **2014**, *4*, 6467−6474.
(21) Wu, F.; Lee, J. T.; Magasinski, A.; Kim, H.; Yushin, G. *Part. Part. Syst. Char.* **2014**, *31*, 639−644.
(22) Nan, C. Y.; Lin, Z.; Liao, H. G.; Song, M. K.; Li, Y. D.; Cairns, E. J. *J. Am. Chem. Soc.* **2014**, *136*, 4659−4663.
(23) Wu, F.; Kim, H.; Magasinski, A.; Lee, J. T.; Lin, H.; Yushin, G. *Adv. Energy Mater.* **2014**, *4*, 1400196−1400203.
(24) Kejie, Z.; Pharr, M.; Vlassak, J. J.; Zhigang, S. *J. Appl. Phys.* **2010**, *108*, 073517.
(25) Hu, L.; Choi, J. W.; Yang, Y.; Jeong, S.; La Mantia, F.; Cui, L.-F.; Cui, Y. *Proc. Natl. Acad. Sci. U.S.A.* **2009**, *106*, 21490−21494.
(26) Wang, C.; Su, K.; Wan, W.; Guo, H.; Zhou, H.; Chen, J.; Zhang, X.; Huang, Y. *J. Mater. Chem. A* **2014**, *2*, 5018−5024.
(27) Liu, H.; Zhang, L.; Guo, Y.; Cheng, C.; Yang, L.; Jiang, L.; Yu, G.; Hu, W.; Liu, Y.; Zhu, D. *J. Mater. Chem. C* **2013**, *1*, 3104−3109.
(28) Aurbach, D.; Pollak, E.; Elazari, R.; Salitra, G.; Kelley, C. S.; Affinito, J. *J. Electrochem. Soc.* **2009**, *156*, A694−A702.
(29) Diao, Y.; Xie, K.; Xiong, S. Z.; Hong, X. B. *J. Power Sources* **2013**, *235*, 181−186.
(30) Fu, Y. Z.; Su, Y. S.; Manthiram, A. *Adv. Energy Mater.* **2014**, *4*, 1300655−1300660.
(31) Han, K.; Shen, J. M.; Hayner, C. M.; Ye, H. Q.; Kung, M. C.; Kung, H. H. *J. Power Sources* **2014**, *251*, 331−337.

■ NOTE ADDED AFTER ASAP PUBLICATION

This paper was published on the Web on February 5, 2015. A new movie file was added to the document, and the paper was reposted on February 11, 2015.

DOI: 10.1021/acs.nanolett.5b00112
Nano Lett. XXXX, XXX, XXX−XXX